Electrochimica Acta 527 (2025) 146267

Contents lists available at ScienceDirect

Electrochimica Acta

journal homepage: www.journals.elsevier.com/electrochimica-acta

Effect of different titanium dioxide (TiO_2) deposition layers for dye-sensitized solar cell (DSSC) application

Nur Alfarina Pirdaus [a,b], Nurfadzilah Ahmad [a,*], Firdaus Muhammad-Sukki [a,c,*], Wan Abd Al Qadr Imad Wan-Mohtar [a,d]

[a] Solar Research Institute (SRI), Universiti Teknologi MARA (UiTM), 40450 Shah Alam, Selangor, Malaysia
[b] School of Electrical Engineering, College of Engineering, Universiti Teknologi MARA (UiTM), 40450 Shah Alam, Selangor, Malaysia
[c] School of Computing, Engineering & the Built Environment, Edinburgh Napier University, EH10 5DT, Edinburgh, United Kingdom
[d] Functional Omics and Bioprocess Development Laboratory, Institute of Biological Sciences, Faculty of Science, Universiti Malaya, 50603 Kuala Lumpur, Malaysia

ARTICLE INFO

Keywords:
Dye-sensitized solar cells
Oyster mushroom dyes
Titanium dioxide deposition layer
Electrical properties
Characterisation

ABSTRACT

Dye-sensitized solar cell (DSSC) is a new type of solar cell that has attracted interest due to its ability to convert energy at a low cost, with simple fabrication, and non-toxic nature. Utilisation of oyster mushroom dye as a natural dye for DSSC is attributed to their large biomass yield and the fact that they can be cultivated in a regulated environment. The TiO_2 pH6 was then used to study different deposition layer thicknesses of TiO_2 thin film (1 layer, 2 layers, 3 layers, 4 layers and 5 layers) to suggest the optimised TiO_2 condition. The characterization of the structural, morphological, optical, and electrical properties of the TiO_2 photoanode with mushroom dye was carried out using XRD, FESEM, AFM, UV–Vis, and I-V measurements in this study, respectively. It was found that the pink oyster mushroom, dried by freeze drying with a 1:10 dilution and pH6 TiO_2 with 3 deposition layers, established the best results in the solar cell performance with efficiency of 0.107 % along with the optimum bandgap of 1.50 eV and anatase structural phase of (101)-planes.

1. Introduction

Research has proven that global energy production could be significantly affected by the impacts of climate change. This situation, along with the increased global demand for electricity, might affect the ability of power plants around the world to produce sufficient energy. Several studies have also proposed that the longest feasible period of non-renewable energy utilisation could only extend up to 2040. Hence, emphasising the need for compulsory actions and the adequate procurement of flexible renewable energy sources is essential to sustain energy production [1]. The deficiency of energy reserves and the harmful effects of burning coal and fossil fuels are the major reasons for the substitution with renewable energy [2]. Non-renewable sources have a few other shortcomings, including air pollution, soil contamination, and land scarcity [3]. Solar cells that can generate electricity directly from sunlight have attracted significant research interest as a potential solution to the energy crisis and related environmental challenges, while advancing sustainable and green energy technologies [4].

Solar energy is poised to become economically viable in the coming years and to expand as an enhanced technology in terms of cost and applications due to the scarcity of non-renewable energy sources. Approximately 1366 W of sunlight reaches the Earth, and this is considered a limitless supply of energy that is readily accessible. The direct conversion of sunlight into solar energy using only the simplest photovoltaic (PV) solar cells is one of solar energy's crucial benefits over other mainstream power sources. Numerous studies have been conducted to produce solar cells with high energy conversion rates in order to incorporate the sun's energy effectively. The main advantage of solar energy over various fossil fuels and oils in prior years is that it is readily available in large quantities. In contrast to conventional energy production methods, solar energy also requires a lesser cost of labour [5]. According to data from the International Energy Agency (IEA), the reservoirs for fossil fuels and coal-based energy sources can persist for up to 29 years and 41 years, respectively [6]. Meanwhile, some studies have indicated that the maximum amount of non-renewable energy use might only last until 2040, which prompted a requirement to find an appropriate and adaptable renewable source to support energy production [1].

* Corresponding authors.
E-mail addresses: nurfadzilah6344@uitm.edu.my (N. Ahmad), f.muhammadsukki@napier.ac.uk (F. Muhammad-Sukki).

https://doi.org/10.1016/j.electacta.2025.146267
Received 19 September 2024; Received in revised form 17 April 2025; Accepted 17 April 2025
Available online 18 April 2025

Considering solar energy produces clean energy and has no negative effects on the environment, it is a viable renewable energy source [7]. Hence, there is a lot of opportunity for solar energy research, particularly in equatorial nations like Malaysia. Since the sun provides the Earth with the equivalent of its annual energy requirement (1.75×10^{17} W) in just one hour, it is theoretically possible for the sun to generate energy to partially meet the world's energy needs using solar technology. Third-generation solar cells, which are based on this technology, have prioritised efficiency optimisation and production cost reduction. This generation of PV technology includes hot carrier cells, polymer solar cells, quantum dot solar cells, dye-sensitised solar cells (DSSCs), heterojunction solar cells, and multi-junction cells [8]. DSSCs have attracted interest in PV technology because of their capacity to convert energy at a low cost. The utilisation of naturally occurring, inexpensively produced, non-toxic, and ecologically friendly pigments may eventually take the place of costly chemical synthesis techniques [9].

Due to their low cost of manufacturing, ease of fabrication, and relatively increasing photo-conversion efficiency, DSSCs have been the subject of extensive research over the past few decades. The components of DSSCs include a counter electrode, an electrolyte solution with a reduction-oxidation process, and dye-sensitised semiconductor photoanodes. The photo-sensitizer, which efficiently absorbs photons and transforms them into electrons, is largely responsible for the DSSCs' performance. The semiconductor is subsequently given the excited charge carriers. The dye's absorption and anchoring on the surface of titanium dioxide (TiO_2) have a significant impact on the effectiveness of the cells. Due to their high conversion efficiency, transition metal coordination compounds, predominantly ruthenium and osmium complexes, are used in the majority of conventional DSSCs as effective sensitizers. However, their use in large-scale fabrication raises serious concerns due to their tedious and time-consuming complex synthesis process as well as their high cost [10]. Despite the fact that higher plants provide the majority of the pigments used for this purpose, there are potential substitute sources that have not been fully utilised but have produced intriguing results. Additionally, organisms including bacteria, cyanobacteria, microalgae, yeast, and moulds, which may be grown in bioreactors or improved by biotechnological methods, can produce useful pigments [9].

2. Methodology

2.1. Preparation of mushroom dye

The fruiting bodies of pink (*Pleurotus djamor*) and yellow (*Pleurotus citrinopileatus*) mushrooms were crushed with a homogenizer and then suspended in 1.5 mol/L NaOH (25 °C) at a volume ratio of 1:30 (mushroom mash/NaOH solution) in order to extract the mushroom dye. To ensure a complete extraction, the suspension was incubated for 80 min in an 80 W sonicator (Fisher Scientific, USA). Following that, the leftover components were eliminated by centrifugation for 15 min at 10,000 rpm. A 7 mol/L HCl solution was added to the supernatant in an Erlenmeyer flask to lower its pH to 1.5. At room temperature, the supernatant was left to precipitate for 3 hr. They were recovered and cleaned with deionized water until the pH reached neutral after the precipitate was centrifuged for 15 min at 10,000 rpm. Ultimately, the raw pigments were extracted and dried in a freeze dryer (Delta 1–24 LSC, Germany) through freeze drying.

2.2. Preparation of TiO_2 nanoparticles by sol-gel method

The reagents used are all analytical grade, and have not been further purified. To create the sol-gel synthesised TiO_2, 10 ml of titanium (IV) butoxide was dissolved in 10 ml of absolute ethanol and agitated for an hour. 5 ml of distilled water was then gradually added dropwise to the solution. Almost instantly, the ensuing gel was created, and it was stirred for a few minutes. The solution was rapidly stirred for an hour to generate white colloidal precipitate after the pH has been corrected with 1 mol of NaOH or HCl for pH6 of the solution. After 24 h, the solutions were filtered. In order to evaporate as much water and organic material as possible, they were then placed in an oven set at 100 °C for the final 12 h. After drying, the material was milled into a fine powder using ball mill machine for 2 h.

2.3. Substrate cleaning process

In this work, fluorine-doped tin oxide (FTO) glass was utilised as the substrate. FTO glass was selected because it has a conductive layer that acts as an electrode. The substrates needed to be thoroughly cleaned before the deposition process could begin. The purpose of the cleaning procedure was to get rid of any contaminants that could have caused the deposited thin film to adhere poorly by forming cracks or irregular thickness. The typical cleaning procedure was followed. The substrate was first cleaned using ethanol (C_2H_5OH) and then, using a Hwashin Technology Powersonic 405 ultrasonic cleaner, deionized (DI) water (H_2O, Milli-Q Advantage A10) for 10 min at a time. Subsequently, the DI water was disposed of and the substrate was cleaned with DI water again before Argon (Ar) gas was blown over it to remove any remaining moisture. The inert gas property of argon led to its selection.

3. Preparation of TiO_2 thin film (photoanode)

2 g of the prepared TiO_2 powder was added into 100 ml of ethyl alcohol and stirred for 30 min to form a homogenous TiO_2 paste. Before usage, the solution was kept in the dark. This study utilised the Laurel Model WS-650SZ spin coater. 10 drops of TiO_2 solution were applied to the substrate and 10 min of heating at 100 °C followed. A spin speed of 3000 rpm was used. The process was repeated for 2 and up to 5 times, representing the number of deposited TiO_2 thin film. After the drying process completed, the deposited thin layer was annealed for 30 min at 500 °C. One parameter that was changed for this procedure was the number of deposition layers, which ranged from 1 to 5 layers.

4. Assembly of DSSC

The DSSC was put together by attaching the platinum counter electrode and the FTO/TiO_2-dye cast with electrolyte. The anode and cathode electrodes were placed on the coated sides using binder clips, and a drop of electrolyte was injected between them through the drilled hole before analysis. The connections were positioned slightly off-centre (for the crocodile clips). The voltage across each cell was measured by shining sunlight or a light source on the cells. The solar simulator was used to characterise electrical parameters such as fill factor (*FF*), efficiency (η), short circuit current (I_{sc}), open-circuit voltage (V_{oc}), current density-voltage (*J-V* curve).

5. Results and discussion

5.1. Electrical properties

The current-voltage (I-V) measurements of sol-gel synthesized TiO_2 thin films for different deposition layers characterised using a Keithley 2600 Two-Point Probe are shown in Fig. 1. TiO_2 is deposited on glass substrate at different deposition layer from 1 to 5 layers with constant annealing temperature of 500 °C. The symmetrical and linear shape of the graph in Fig. 1 implies that the TiO_2 thin film and the gold (Au) metal contact possess ohmic contact characteristics [11]. The slope of the curve is observed to increase with the increase in deposition layer. Five deposition layers show the steepest slope followed by four layers, three layers, two layers and one layer. However, one deposition layer exhibited the highest maximum current (2.3591×10^{-9} A) while two layers showed the lowest maximum current (2.005×10^{-9} A) at 10 V.

Resistivity, ρ was calculated from the current-voltage (I-V) curve

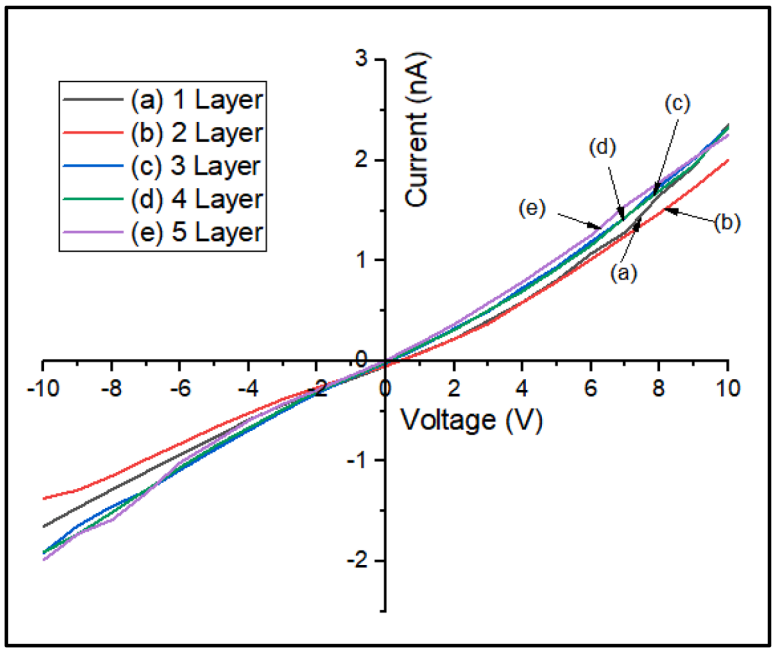

Fig. 1. I-V measurement plots of TiO_2 thin films with 5 different deposition layers. (a) 1 layer (b) 2 layers (c) 3 layers (d) 4 layers (e) 5 layers.

obtained using Eq. (1) while conductivity, σ was calculated using Eq. (2). The Keithley 2600 two-point probe characterisation system, connected to a room-temperature probe station, can be used to characterise electrical properties such as resistivity, conductivity and ohmic or Schottky behaviour on the TiO_2 thin film. Determining the electrical characteristics of the materials used to make solar cells is crucial. The thin film's conductivity and resistivity were examined in this work. The voltage range used to measure the electrical behaviour was −10 V to 10 V.

$$\rho = \left(\frac{V}{I}\right)\left(\frac{wt}{L}\right) \tag{1}$$

where V is the voltage supplied, I is the current measured in ampere (A), t is the thickness of the film measured using Scanning Electron Microscope in micrometer (μm) using 4000 ×, w is the Au electrode width in meter while L is the length between two Au electrode in meter (m). Conductivity, σ was calculated using Eq. (2):

$$\sigma = \frac{1}{\rho} \tag{2}$$

The trend for resistivity (Fig. 2) and conductivity (Fig. 3) is observed to be inversely proportional to the thickness of the deposition layer. As the thickness of TiO_2 deposition layer increases, the resistivity also increases from 5.454×10^3, 12.143×10^3, 34.660×10^3, 41.203×10^3 and 46.121×10^3 Ω.m for 1, 2, 3, 4 and 5 layers respectively. The conductivity decreases as the deposition layer increases from 18.34×10^{-5}, 8.235×10^{-5}, 2.885×10^{-5}, 2.427×10^{-5} and 2.168×10^{-5} $S.m^{-1}$ for 1, 2, 3, 4 and 5 layers respectively.

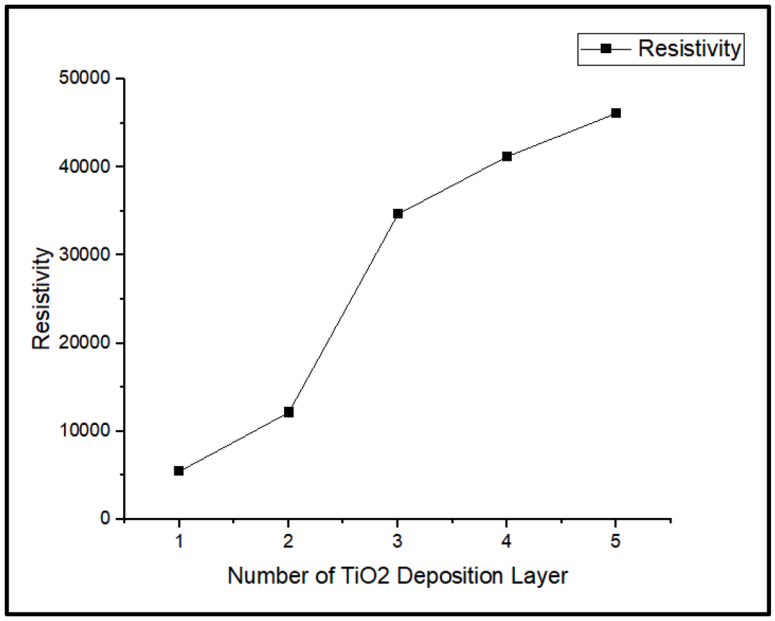

Fig. 2. Resistivity of TiO_2 photoanodes with 5 different deposition layers.

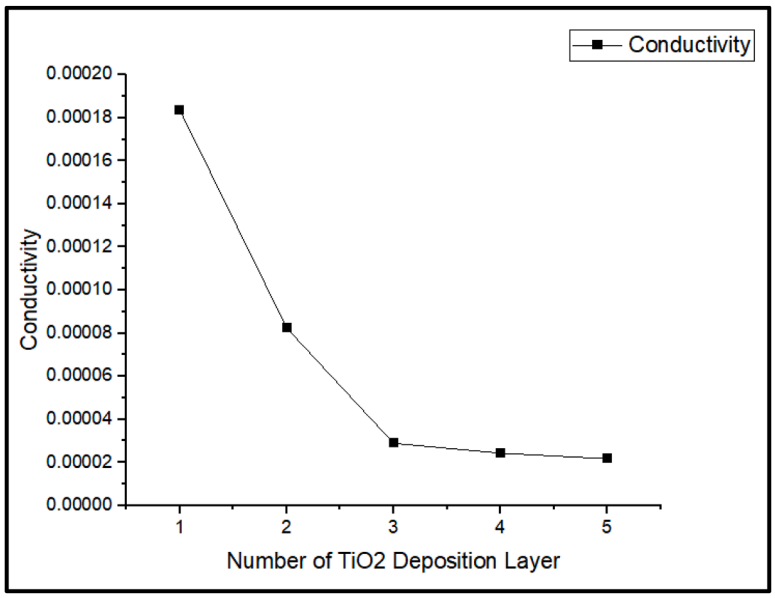

Fig. 3. Conductivity of TiO_2 photoanodes with 5 different deposition layers.

Table 1 summarises the data of thickness, resistance, resistivity and conductivity for 5 deposition layers of TiO_2 photoanodes.

5.2. Optical properties

The optical transmittance spectra for TiO_2 thin film samples with different deposition layers are shown in Fig. 4. The transmittance of the five samples shows an increasing transmittance with only a small increase. Single deposition layer of TiO_2 shows the highest transmittance compared to the other four thicker deposition layers with 40 % transmittance. Meanwhile, two, three, four and five deposition layers only exhibit transmittance below 10 %. Transmittance values decrease as film thickness increases. The decrease in transmittance with increasing film thickness is related to free carrier absorption and photon scattering because of the rougher surface of the film [12]. Low transmittance might be due to the dense and compact structure of the TiO_2 film's crystalline structure which reduces its transparency.

Fig. 4(a)–(d) show the UV–visible optical transmittance spectra of the TiO_2 films with different thicknesses between 300 and 800 nm in wavelength. All films have high transmittance, and the absorption edge is at about 300 nm. In addition, the transmittance of the films becomes lower as the films become thicker. The average transmittance of the film (a), (b) (c) and (d) in the visible range was about 85 %, 80 %, 75 % and 60 %, respectively [13].

Fig. 5 represents the absorption coefficient of TiO_2 thin film samples with different deposition layers which is defined by the obtained transmittance spectra shown in Fig. 4 in the wavelength of 300–800 nm. A higher absorption coefficient may result from the semiconducting layer becoming thicker because a thick layer increases the potential for absorption by providing more opportunity for light to interact with the material. The electron transit within the cell is also influenced by the semiconducting layer's thickness. Longer electron diffusion lengths could be achieved via a thicker layer, although recombination losses might also rise as a result. As a result, there is a trade-off between charge transfer optimisation and light absorption maximisation [13]. The characteristics of the dye sensitizer utilised in the DSSC also have an impact on the absorption coefficient. However, the spectrum of the film shows increased absorbance at about 300 nm and a small absorbance at around 450 nm, indicating the increased dye loading amount, which can drastically increase effective light absorption [14]. The dye molecule does not completely get absorbed at the inner surface of porous TiO_2 film when the particle size in TiO_2 film with Ti-layer is comparable with the interparticle distance in the porous TiO_2. However, in our study due to the large particle size the dye molecule penetration is much more feasible into the porous TiO_2 layer, thereby favouring more dye adsorption [14].

Table 1
Data of thickness, resistance, resistivity and conductivity for 5 deposition layers of TiO_2 photoanodes.

Number Layer	Thickness Layer (nm)	Resistance (Ω)	Resistivity (Ω.m)	Conductivity (S. m^{-1})
1	220	5.526×10^9	5.454×10^3	18.34×10^{-5}
2	690	6.227×10^9	12.143×10^3	8.235×10^{-5}
3	1160	5.033×10^9	34.660×10^3	2.885×10^{-5}
4	1250	5.054×10^9	41.203×10^3	2.427×10^{-5}
5	1600	4.933×10^9	46.121×10^3	2.168×10^{-5}

Beer's law was used to estimate the optical band gap energy (*Eg*) based on the absorbance spectra obtained from UV–Vis-NIR characterisation and the Tauc plot was used to calculate the *Eg* using Eq. (3):

$$\alpha h\nu = A(h\nu - Eg)^n \quad (3)$$

It was estimated by extrapolating the linear portion of $(\alpha h\nu)^2$ vs photon energy curve to the photon energy axis, respectively [15].The Tauc plot of TiO_2 thin films produced at various deposition layers is shown in Fig. 6. The bandgap energy for 1 layer, 2 layers, 3 layers, 4 layers and 5 layers are 1.55 eV, 1.50 eV, 1.50 eV, 1.48 eV and 1.49 eV respectively. Theoretically, optical bandgap values are supposed to decrease with increasing film thickness, which is due to the addition of new energy levels near the valence band inside the energy gap brought about by the increase in film thickness. This condition creates bridges for the electrons (with lower energies than the energy gap value for the first thin film) transmitted between the valence band and the conduction band, increasing the quantity of electron transfers and altering the Fermi level. Due to reaching the lowest bandgap energy in this instance, the 3-layer TiO_2 deposition layer thin film shows the largest number of electrons that can be transferred [16]. This condition might be due to the quantum confinement effect which has an impact on the bandgap energy of some materials, particularly semiconductors. The spatial confinement of electrons and holes within a semiconductor material increases with decreasing material thickness. The quantisation of energy levels brought about by this confinement can raise the bandgap energy. Therefore,

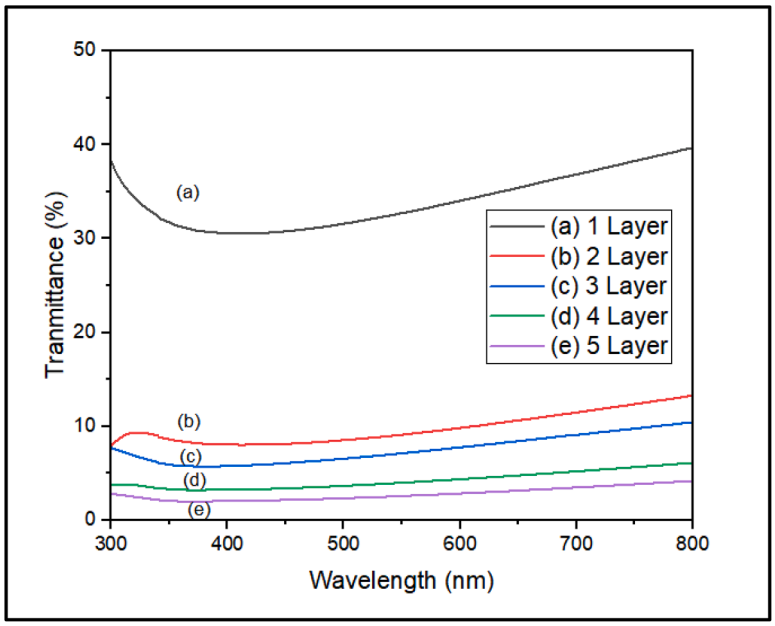

Fig. 4. Transmittance spectra of TiO_2 photoanodes with 5 different deposition layers. (a) 1 layer (b) 2 layers (c) 3 layers (d) 4 layers (e) 5 layers.

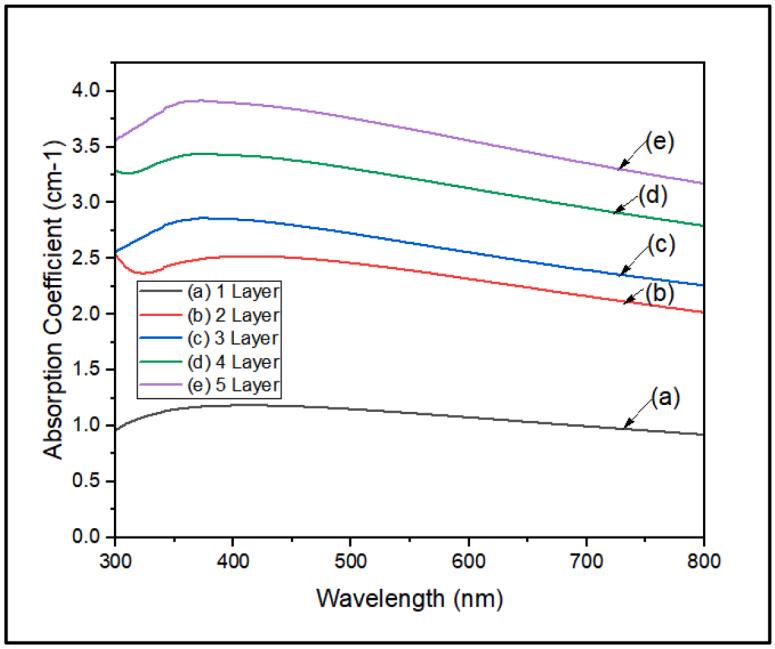

Fig. 5. Absorption coefficient of TiO_2 photoanodes with 5 different deposition layers (a) 1 layer (b) 2 layers (c) 3 layers (d) 4 layers (e) 5 layers.

titanium coating improves the crystalline arrangement of TiO_2 film in the anatase nature, which makes it suitable for PV application [14]. On the other hand, it was also discovered that polyvinyl alcohol (PVA) nanocomposite is reported to have the smallest particle because the Anatase structure increases the conjugation of the PVA matrix. Thus, the Anatase phase structure is preferred over the Rutile phase by its higher electron mobility, which leads to a decrease in the nanocomposite's optical energy gap PVA-Rutile nanocomposite illustrates the greatest one [17]. A thicker film can trap more light, resulting in a lower transmittance and a higher absorbance value. This is because a thicker film allows light to enter through it on a longer journey. The measurement's results demonstrate that thickness might have a significant impact on TiO_2 photoanode optical characteristics.

6. Structural properties

Structural properties of TiO_2 thin films with different layers of deposition were studied using X-ray Diffraction (XRD) analysis ranging the 2theta of 10° to 90°. From the XRD pattern obtained, one potential peak of anatase was formed at 25° with the increase in intensity of the peak as the thickness of TiO_2 layer increased from 2 layers (Fig. 7(b)) to 5 layers (Fig. 7(e)). A single deposition layer (a) of TiO_2 only exhibited a broad peak, indicating an amorphous layer. This potential peak of anatase in sample (b) to (e) observed from the spectra supposed to belong to (101)-planes of anatase phase. We obtained the anatase phase for the TiO_2 powder synthesised with pH6 and proceeded with the optimised pH for photoanode preparation.

When the film thickness increased, the peaks of the (101)-plane for

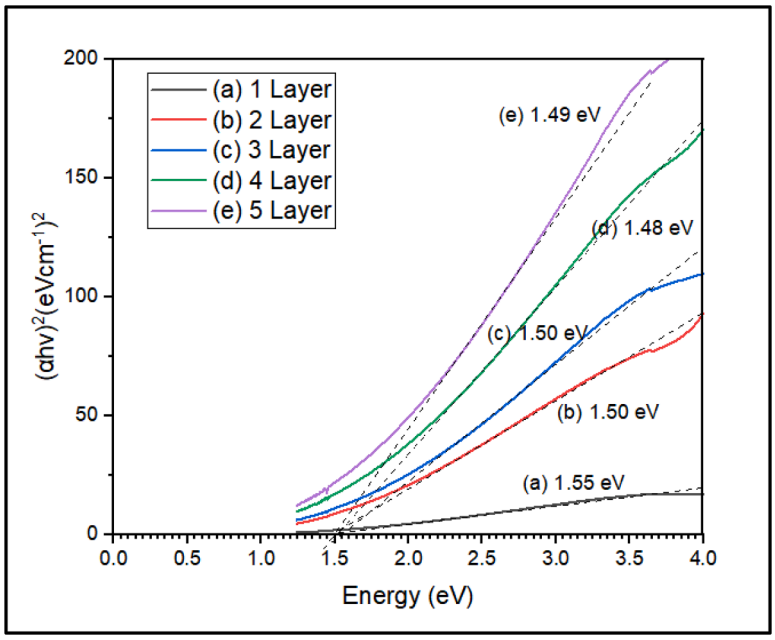

Fig. 6. Tauc plot of TiO_2 photoanodes with 5 different deposition layers. a) 1 layer (b) 2 layers (c) 3 layers (d) 4 layers (e) 5 layers.

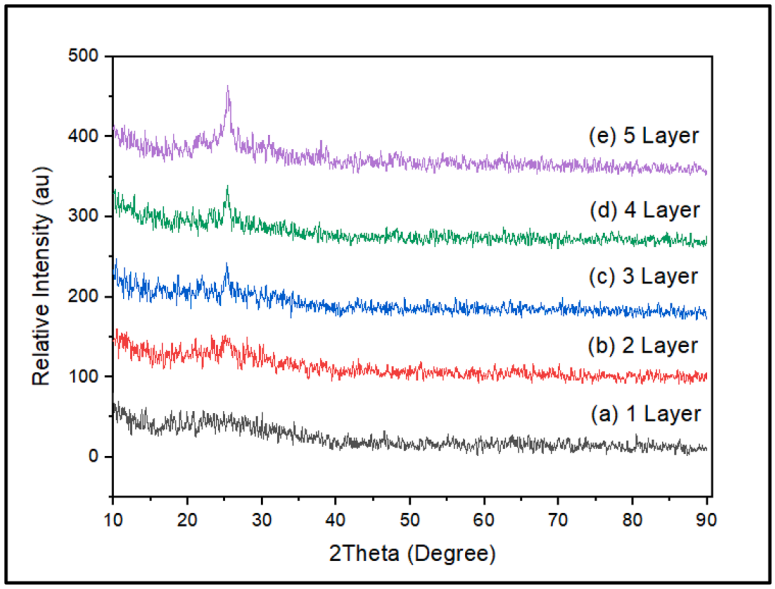

Fig. 7. XRD spectra of 5 deposition layers of TiO_2 photoanodes. a) 1 layer (b) 2 layers (c) 3 layers (d) 4 layers (e) 5 layers.

the samples sharpened, indicating the enhancement of crystallinity. The (101) peaks of TiO_2 films displayed a clear alignment of the (101)-axis with the substrate surface [13]. These results demonstrated that TiO_2 film structure improves with increasing film thickness. The observed intensity exhibited a direct proportionality to the film thickness. This may be attributed to the expansion of the atomic layer as the number of layers (thickness) increased. In their study, Goncalves et al. found that a denser film contains a greater number of atomic layers that scatter X-rays [18]. TiO_2 suggests that a 400 °C heat treatment might convert the rutile phase into the anatase phase, in accordance with prior studies [19]. A 500 °C heat treatment was utilised for annealing temperature in this study. From the results obtained by various characterisations of the thickness of TiO_2 photoanode, an optimum DSSC device was fabricated with the optimum TiO_2 of pH6 and 3 deposition layers.

7. Application of the optimised properties on DSSC's efficiency

The Newport Oriel Sol3A solar simulator was used to characterise the current-voltage (I-V) characteristics of the manufactured DSSC under AM 1.5 sun conditions (100 mW/cm^2, 25 °C). The manufactured FTO/TiO_2-PFOM/electrolyte/Pt with a sample size of 1 × 1 cm^2 showed a V_{oc} of 0.499 V, an I_{sc} of 1.987 × 10–5 mA/cm^2, and J_{sc} of 0.397 mA/cm^2 according to the results from the solar simulator (see Fig. 8). Further analysis can be found in [20].

The device's fill factor, FF, was determined using the following Eq. (4):

$$FF = \frac{(Vmax \times Jmax)}{(Voc \times Jsc)} \tag{4}$$

where J_{sc} is the short circuit current density, which is the maximum

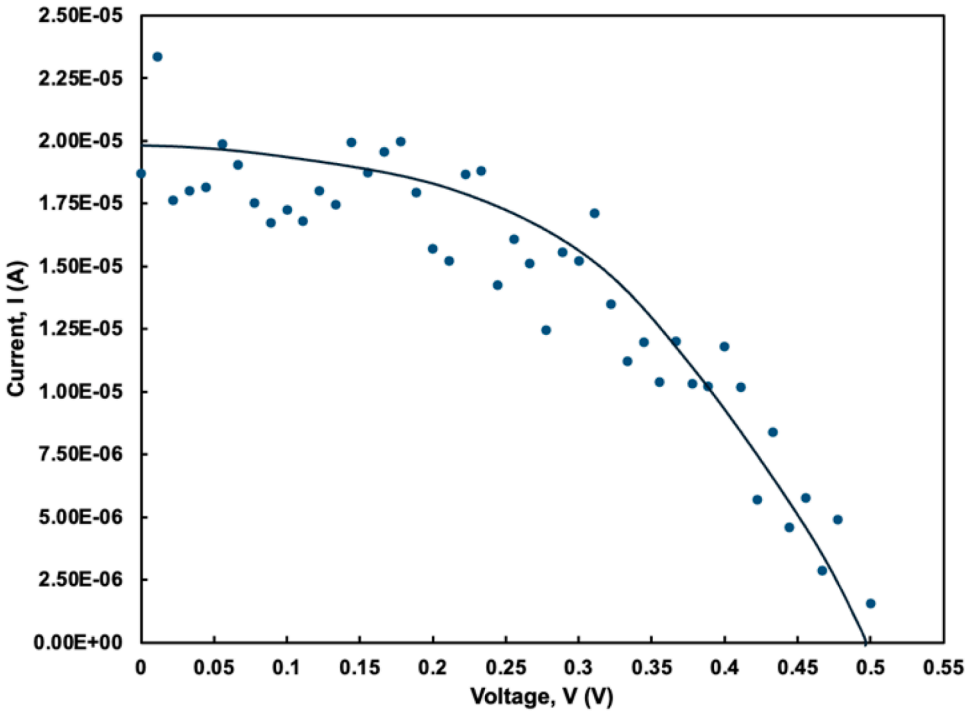

Fig. 8. I-V Characteristics for FTO/TiO_2-PFOM/electrolyte/Pt.

current that exists when the voltage across the device is zero, and V_{max} and J_{max} are the maximum values of the voltage and current, respectively. V_{oc} is the open circuit voltage, which occurs when the maximum current occurs when the voltage across the device is zero. The following Eq. (5) determines the power conversion efficiency, η, while P_{inc} is the radiation power incident on the cell:

$$\eta = \frac{Jsc \times Voc \times FF}{Pinc} \quad (5)$$

The overall efficiency of the cell is 0.107 %, and the performance of the manufactured device was assessed using the results from the solar simulator with *FF* of 53.756. The results were summarised in Table 2 below.

The fabricated DSSC attained is within the range of the DSSC that was previously produced utilising a different source of fungal dye, *Cortinarius* fungi, which recorded $V_{oc} = 541$ mV, $J_{sc} = 1.79$ mA/cm^2, $FF = 65$, and $\eta = 0{,}64$ %. The inadequate electron injection procedure and the device's limited ability to absorb light in the visible spectrum could be the cause of its low efficiency. Low DSSC efficiency of natural dyes is typically caused by low energy of the dye excited state, rapid recombination of dye molecules, and chemicals in the extracts that promote cellular recombination in the cells [21].

The low extinction coefficient value and lack of or diminished bonding to the TiO_2 are the causes of the lower conversion efficiency. Therefore, improved absorption in the solar cell's visible region and efficient electron transport are responsible for the better efficiency of the device. The two important factors in assessing the cell's efficiency are the J_{sc} and V_{oc} [22].

8. Conclusion

The study proposed a novel natural dye extracted from pink oyster mushroom (*P. djamor*) to be embedded as the photosensitizer along the optimum thickness for TiO_2 coating on the glass substrate. The characterisation was analysed to study the effects of the deposition layer thickness on the morphological, structural, optical, and electrical properties of the TiO_2 thin films for DSSC application. The results demonstrate that current-voltage (I-V) characteristics exhibited ohmic contact with the Au metal contact with the increasing slope as the thickness increased. Resistivity also increased along with increase in the thickness, and this is the opposite for conductivity. Optical, structural and morphological properties supported the results in deciding 3 deposition layers as the optimum thickness for TiO_2 photoanode.

Table 2
Data of short-circuit current, open-circuit voltage, fill factor and efficiency of fabricated DSSC.

Short-circuit Current, I_{sc} (mA)	Open-circuit Voltage, V_{oc} (V)	Fill Factor, *FF*	Efficiency, η (%)
1.987×10^{-5}	0.499	53.756	0.107

CRediT authorship contribution statement

Nur Alfarina Pirdaus: Conceptualization, Data curation, Formal analysis, Investigation, Methodology, Visualization, Writing – original draft, Writing – review & editing. **Nurfadzilah Ahmad:** Conceptualization, Formal analysis, Funding acquisition, Investigation, Methodology, Project administration, Resources, Software, Supervision, Validation, Writing – review & editing. **Firdaus Muhammad-Sukki:** Conceptualization, Formal analysis, Funding acquisition, Investigation, Methodology, Project administration, Resources, Validation, Visualization, Writing – review & editing. **Wan Abd Al Qadr Imad Wan-Mohtar:** Conceptualization, Formal analysis, Funding acquisition, Investigation, Methodology, Project administration, Resources, Supervision, Validation, Writing – review & editing.

Declaration of competing interest

The authors declare that they have no known competing financial interests or personal relationships that could have appeared to influence the work reported in this paper.

Acknowledgements

N.A. would like to thank Universiti Teknologi MARA (UiTM) under FRGS: 600-RMC/FRGS5/3 (119/2021); W.A.A.Q.I.W.-M. acknowledges PETRONAS Research Sdn Bhd under PV055–2022; and F.M.-S. recognises the Royal Society of Edinburgh through RSE Personal Research Fellowship Grant (Project ID: 3204).

References

[1] J. Solé, A. García-Olivares, A. Turiel, J. Ballabrera-Poy, Renewable transitions and the net energy from oil liquids: a scenarios study, Renew Energy 116 (2018) 258–271, https://doi.org/10.1016/j.renene.2017.09.035.
[2] A. Bhagavatula, "Thermo-chemical conversion of coal-biomass blends: kinetics modeling of pyrolysis, moving bed gasification and stable carbon isotope analysis," 2014.
[3] F. Perera, Pollution from fossil-fuel combustion is the leading environmental threat to global pediatric health and equity: solutions exist, in eng, Int. J. Environ. Res. Public Health 15 (1) (2017), https://doi.org/10.3390/ijerph15010016.
[4] Y. Huang, E.J. Kramer, A.J. Heeger, G.C. Bazan, Bulk heterojunction solar cells: morphology and performance relationships, Chem. Rev. 114 (14) (2014) 7006–7043, https://doi.org/10.1021/cr400353v.
[5] M.S. Shaikh, A review paper on electricity generation from solar energy, Int. J. Res. Appl. Sci. Eng. Technol. (2017) 1884–1889.
[6] M. Samsudin, M.M. Rahman, M. Wahid, Power generation sources in Malaysia: status and prospects for sustainable development, J. Adv. Rev. Scientific Res. 25 (2016) 2289–7887.
[7] O. Ellabban, H. Abu-Rub, F. Blaabjerg, Renewable energy resources: current status, future prospects and their enabling technology, Renew. Sustain. Energy Rev. 39 (2014) 748–764, https://doi.org/10.1016/j.rser.2014.07.113.
[8] P.P. Kumavat, P. Sonar, D.S. Dalal, An overview on basics of organic and dye sensitized solar cells, their mechanism and recent improvements, Renew. Sustain. Energy Rev. 78 (2017) 1262–1287, https://doi.org/10.1016/j.rser.2017.05.011.
[9] N. Eriksen, Production of phycocyanin - A pigment with applications in biology, biotechnology, foods and medicine, Appl. Microbiol. Biotechnol. 80 (2008) 1–14, https://doi.org/10.1007/s00253-008-1542-y.
[10] A. Arulraj, G. Senguttuvan, S. Veeramani, V. Sivakumar, B. Subramanian, Photovoltaic performance of natural metal free photo-sensitizer for TiO_2 based dye-sensitized solar cells, Optik (Stuttg) 181 (2019) 619–626, https://doi.org/10.1016/j.ijleo.2018.12.104.
[11] H.M. Faruk, P.M. Sarwar, N.M.A. I, Influence of film thickness on optical and morphological properties of TiO_2 thin films, Emerg. Mater. Res. 9 (1) (2020) 186–191, https://doi.org/10.1680/jemmr.17.00085.
[12] M.C. Kao, H.Z. Chen, S.L. Young, C.Y. Kung, C.C. Lin, The effects of the thickness of TiO_2 films on the performance of dye-sensitized solar cells, Thin. Solid. Films 517 (17) (2009) 5096–5099, https://doi.org/10.1016/j.tsf.2009.03.102.
[13] M.K. Das, N.S. Chickerur, Fabrication of polycrystalline silicon solar cells showing high efficiency, Bull. Mater. Sci. 21 (6) (1998) 475–478, https://doi.org/10.1007/BF02790349.
[14] D.W. Bruce, D. O'Hare, R.I. Walton, *Energy Materials* (Inorganic Materials Series), United Kingdom: Wiley, 2011.
[15] R.J. Beula, S. Devadason, V.M. Kumar, Effect of titanium coating on the structural and optical properties of TiO_2 thin films for improved performance in dye-sensitized solar cells, in: International Conference on Recent Trends in Materials Science and Applications (ICRTMSA), Tiruchirappalli, INDIA 189, Springer Proceedings in Physics, 2017, pp. 437–449, https://doi.org/10.1007/978-3-319-44890-9_40, 2016.
[16] K. Priyalakshmi Devi, P. Goswami, H. Chaturvedi, Fabrication of nanocrystalline TiO_2 thin films using Sol-Gel spin coating technology and investigation of its structural, morphology and optical characteristics, Appl. Surf. Sci. 591 (2022) 153226, https://doi.org/10.1016/j.apsusc.2022.153226.
[17] H.I. Elsaeedy, A. Qasem, H.A. Yakout, M. Mahmoud, The pivotal role of TiO_2 layer thickness in optimizing the performance of TiO_2/P-Si solar cell, J. Alloys Compd. 867 (2021) 159150, https://doi.org/10.1016/j.jallcom.2021.159150.
[18] S. Velu Kuppu, et al., Developments of photo-anode materials for dye-sensitized solar cell using natural sensitizer of Portulaca grandiflora flower soaked Titania nanocrystalline and nanofiber, Chem. Phys. Lett. 812 (2023) 140271, https://doi.org/10.1016/j.cplett.2022.140271.
[19] I. Morad, A.M. Alshehri, A.F. Mansour, M.H. Wasfy, M.M. El-Desoky, Facile synthesis and comparative study for the optical performance of different TiO_2 phases doped PVA nanocomposite films, Physica B 597 (2020) 412415, https://doi.org/10.1016/j.physb.2020.412415.
[20] N.A. Pirdaus, et al., Performance of yellow and pink oyster mushroom dyes in dye sensitized solar cell, Scientific Reports 2024 14:1 14 (1) (2024) 1–19, https://doi.org/10.1038/s41598-024-73865-z.
[21] M. Addamo, et al., Photocatalytic thin films of TiO_2 formed by a sol–gel process using titanium tetraisopropoxide as the precursor, Thin. Solid. Films 516 (12) (2008) 3802–3807, https://doi.org/10.1016/j.tsf.2007.06.139.
[22] M. Lal, P. Sharma, C. Ram, Synthesis and photocatalytic potential of Nd-doped TiO_2 under UV and solar light irradiation using a sol-gel ultrasonication method, Results Mater. 15 (2022) 100308, https://doi.org/10.1016/j.rinma.2022.100308.